A&A 627, A178 (2019)
https://doi.org/10.1051/0004-6361/201834391

Astronomy & Astrophysics

H-band discovery of additional second-generation stars in the Galactic bulge globular cluster NGC 6522 as observed by APOGEE and *Gaia*

J. G. Fernández-Trincado[1,2,3], O. Zamora[4,5], Diogo Souto[6,7], R. E. Cohen[8], F. Dell'Agli[4,5], D. A. García-Hernández[4,5], T. Masseron[4,5], R. P. Schiavon[9], Sz. Mészáros[10]⋆, K. Cunha[11,6], S. Hasselquist[12], M. Shetrone[13], J. Schiappacasse Ulloa[3], B. Tang[14], D. Geisler[3,15,16], D. R. G. Schleicher[3], S. Villanova[3], R. E. Mennickent[3], D. Minniti[17,18,19], J. Alonso-García[20,18], A. Manchado[4,5,21], T. C. Beers[22], J. Sobeck[23], G. Zasowski[24], M. Schultheis[25], S. R. Majewski[26], A. Rojas-Arriagada[27], A. Almeida[15], F. Santana[28], R. J. Oelkers[29], P. Longa-Peña[20], R. Carrera[4,5], A. J. Burgasser[30], R. R. Lane[27], A. Roman-Lopes[15], I. I. Ivans[24], and F. R. Hearty[31]

(Affiliations can be found after the references)

Received 5 October 2018 / Accepted 13 June 2019

ABSTRACT

We present an elemental abundance analysis of high-resolution spectra for five giant stars spatially located within the innermost regions of the bulge globular cluster NGC 6522 and derive Fe, Mg, Al, C, N, O, Si, and Ce abundances based on *H*-band spectra taken with the multi-object APOGEE-north spectrograph from the SDSS-IV Apache Point Observatory Galactic Evolution Experiment (APOGEE) survey. Of the five cluster candidates, two previously unremarked stars are confirmed to have second-generation (SG) abundance patterns, with the basic pattern of depletion in C and Mg simultaneous with enrichment in N and Al as seen in other SG globular cluster populations at similar metallicity. In agreement with the most recent optical studies, the NGC 6522 stars analyzed exhibit (when available) only mild overabundances of the *s*-process element Ce, contradicting the idea that NGC 6522 stars are formed from gas enriched by spinstars and indicating that other stellar sources such as massive AGB stars could be the primary polluters of intra-cluster medium. The peculiar abundance signatures of SG stars have been observed in our data, confirming the presence of multiple generations of stars in NGC 6522.

Key words. stars: abundances – stars: Population II – globular clusters: individual: NGC 6522 – Galaxy: formation – Galaxy: structure

1. Introduction

Multiple populations (MPs) of stars with distinctive light-element abundances were recently identified in several bulge globular clusters (see, Schiavon et al. 2017a; Recio-Blanco et al. 2017; Tang et al. 2017; Muñoz et al. 2017, for instance). In particular, Schiavon et al. (2017a) studied the chemical composition of a few red giant stars within the bulge globular clusters (GCs) NGC 6553, NGC 6528, Terzan 5, Palomar 6, and NGC 6522 using near infrared (NIR; 1.5–1.7 μm) high-resolution (R = 22 000) APOGEE spectra from the twelfth data release (DR12, Alam et al. 2015). These studies also included the re-reduced and re-calibrated spectra of the latest APOGEE DR13[1] data release (Albareti et al. 2017) for the globular cluster NGC 6553 (e.g., Tang et al. 2017), where we included more chemical species with reliable light-element abundances (namely O, Na, Si, Ca, Cr, Mn, and Ni). Schiavon et al. (2017a) and Tang et al. (2017) provided useful chemical "tags" in several elemental abundances for a number of Milky Way bulge globular cluster stars that exhibit N and Al abundances well above typical Galactic levels at a range of metallicities. In other words, they found distinctive chemical patterns characterizing MPs, with comparable chemical behavior to what is reported in extensive spectroscopic and photometry surveys of GCs in general (see Gratton et al. 2004, 2007, 2012; Carretta et al. 2007, 2009a,b, 2010; Mészáros et al. 2015; García-Hernández et al. 2015; Carretta 2016; Recio-Blanco et al. 2017; Pancino et al. 2017; Schiavon et al. 2017a; Mészáros et al. 2018; Tang et al. 2017; Bastian & Lardo 2018; Tang et al. 2018; Kerber et al. 2018).

Large-scale spectroscopic surveys like APOGEE (see Majewski et al. 2017) have confirmed that several bulge GCs exhibit significant star-to-star abundance variations in their light-element content (see Schiavon et al. 2017a; Tang et al. 2017), with the usual anti-correlations between pairs of light elements, such as C–N and Al–N. This behavior demonstrates that the CNO, NeNa, and MgAl cycles took place in these GCs (see, e.g., Mészáros et al. 2015; Schiavon et al. 2017a; Tang et al. 2017; Pancino et al. 2017; Ventura et al. 2016; Dell'Agli et al. 2018).

Following this line of investigation, we turn our attention to the low-mass (~5.93 × 10^4 $M_\odot$: Gnedin & Ostriker 1997) and old (~12.5 and 13.0 Gyr: Kerber et al. 2018) bulge globular cluster NGC 6522. Earlier studies show that this ancient Milky Way globular cluster hosts remarkably high abundances of slow neutron-capture (*s*-process) elements (e.g., Chiappini et al. 2011). Chiappini et al. (2011) interpreted this observation as evidence of NGC 6522 stars being formed from gas enriched by massive fast-rotating stars (spinstars; see Pignatari et al. 2008), which possibly makes NGC 6522 distinct from other GCs.

⋆ Premium Postdoctoral Fellow of the Hungarian Academy of Sciences.

[1] *APOGEE field – BAADEWIN_001-04*: particularly in this field, APOGEE/DR13/DR14 have the same targets as APOGEE DR12, but the data reduction and calibration have been improved in several ways. For more details we refer the reader to a forthcoming paper (Holtzman et al. in prep.).

However, more recent chemical re-analysis by Ness et al. (2014) and Barbuy et al. (2014) found no enhancement in the *s*-process elements for the same stars previously studied by Chiappini et al. (2011). The abundances they find can be explained by mass transfer from *s*-process-rich asymptotic giant branch (AGB) stars or alternative self-enrichment scenarios (e.g., the massive AGBs self-enrichment scenario) without invoking massive fast-rotating stars. Kerber et al. (2018), based on a detailed analysis of *Hubble* Space Telescope (HST) proper-motion-cleaned color-magnitude diagrams (CMDs), found that NGC 6522 exhibits at least two stellar populations with an intrinsically wide subgiant branch, consistent with a first and second stellar generation.

Here we carry out a detailed re-analysis of the NGC 6522 field to search for abundance anomalies through the line-by-line spectrum synthesis calculations for the full set of (atomic and molecular) lines (particularly CN, OH, CO, Al, Mg, and Si) in the re-reduced APOGEE DR14 spectra (Abolfathi et al. 2018). The phenomenon of star-to-star light-element abundance variations in NGC 6522 indicates the presence of MPs, such as those claimed by Schiavon et al. (2017a) and Recio-Blanco et al. (2017), and provides crucial observational evidence that NGC 6522 could be the fossil relic of one of the structures that contributed to generating the N-rich population towards the Milky Way bulge (Schiavon et al. 2017b). It also reinforces the link between GCs and the chemical anomalies (second-generation field stars[2]) recently found toward the Galactic bulge field (e.g., Fernández-Trincado et al. 2017b, 2019d), as well as that with the N-rich moderately metal-poor halo stars (Martell & Grebel 2010; Martell et al. 2011, 2016; Tang et al. 2019), mimicking the chemical abundance patterns of the second-generation population of globular clusters (see Fernández-Trincado et al. 2016a, 2019a,b,c,d). More recently, observations extending the analysis to other elements have already detected departures from what seemed to be a simple chemical evolutionary path, like the existence of a Na-rich population toward the outer bulge likely originating from disrupted GCs (e.g., Lee et al. 2019).

This article is structured as follows. We describe the data in Sect. 2 and the cluster membership selection in Sect. 3. In Sects. 4 and 5 we provide our abundance analysis for light and heavy elements, respectively, and in Sect. 6 we discuss the results. We present our conclusions in Sect. 7.

2. APOGEE data

High-resolution ($R \sim 22\,500$) H-band spectroscopic ($\lambda = 1.51$–$1.69\,\mu$m) observations were obtained with the APOGEE, as part of Sloan Digital Sky Survey IV that observed 277 000 stars in the Milky Way (see Gunn et al. 2006; Eisenstein et al. 2011; Wilson et al. 2012; Majewski et al. 2017). Here we use the most recenter-reduced and re-calibrated APOGEE spectra from the fourteenth data release of SDSS (DR14, Abolfathi et al. 2018).

We have re-analyzed available APOGEE spectra towards the Baade's window (APOGEE field: BAADEWIN_001-04) region around $(l, b) \approx (1°, -4°)$ with a field of view of ∼3 sq. deg, comprising 460 stars (for details, see Zasowski et al. 2013, 2017).

One of our stars in the BAADEWIN_001-04 field, 2M18032356−3001588, was recently studied in Schiavon et al. (2017a) using the DR12/ASPCAP[3] (García Pérez et al. 2016) datasets. The same authors suggested the presence of MPs in NGC 6522 based on the polluted chemistry (high Al and N) observed in 2M18032356−3001588. This hypothesis has recently been supported by similar analysis from the *Gaia*-ESO survey (see Recio-Blanco et al. 2017). Here we present an independent analysis using the newly released APOGEE DR14 stellar spectra towards NGC 6522, and report the identification of four new potential cluster members with polluted chemistry towards the innermost regions of the cluster.

It is to be noted here that the new highest-likelihood cluster members (four stars) were originally missed by Schiavon et al. (2017a), because they adopted more rigorous limits on the NGC 6522 parameter space (radial velocity, metallicity, $T_{\rm eff}$, etc.) as well as higher restrictions on the signal-to-noise ratio ($S/N > 70\,{\rm pixel}^{-1}$) of the APOGEE spectra. In the following section, we present our adopted softer limits that take into account the updated parameter space of NGC 6522 and that have allowed us to identify new potential cluster members based on APOGEE data.

3. Cluster membership selection

We selected probable cluster members based on the revised version of the structural parameters of NGC 6522, that is, the cluster center $(\alpha, \delta) = (270.896805°, -30.034204°)$, with an uncertainty of 0.3 arcsec, from ellipse fitting to density maps from HST point spread function photometry, and the tidal radius of the cluster: $r_{\rm t} < 7.1^{+6.1}_{-3.7}$ arcmin. For a more detailed discussion, we refer the reader to Cohen et al. (2018).

To select the highest-likelihood cluster members we also adopt a radial velocity range of $\langle {\rm RV} \rangle \sim -21.1 \pm 15\,{\rm km\,s^{-1}}$ (Harris 1996). We have adopted a metallicity range of [Fe/H] ∼ −1.0 ± 0.3 dex (e.g., Barbuy et al. 2009, 2014); our stars are also recovered even adopting the cluster metallicity as reported in Ness et al. (2014): [Fe/H] = −1.15. The radial velocity and metallicity of our stellar sample are displayed in Fig. 1, which shows that most stars have radial velocities and metallicities very close to the mean cluster values.

Figure 2 shows the spatial distribution of four new potential cluster members (2M18033819−3000515, 2M18033965−3000521, 2M18034052−3003281, and 2M18033660−3002164) plotted against one star previously identified on APOGEE (2M18032356−3001588); the four stars clearly lie near the cluster center (all our candidate members fall within a relatively small radius, ∼2.5 arcmin), as illustrated in the same figure. It is important to note that a detailed chemical analysis has not been done so far for these objects, except for: (i) 2M18033660−3002164, which was analyzed in Chiappini et al. (2011) and Ness et al. (2014) from GIRAFFE/VLT spectra. Unfortunately, this is the faintest star in our sample (see Table 1) and its low-S/N APOGEE spectrum does not permit us to carry out a reliable and conclusive abundance analysis, especially for Al I lines; (ii) 2M18032356−3001588, was already studied by Schiavon et al. (2017a, light elements) and Cunha et al. (2017, heavy elements). We note however that we carry out an independent chemical analysis of 2M18032356−3001588 (Schiavon et al. 2017a), which permit us to revisit its chemical composition.

It is instructive to contrast the potential cluster candidate stars with those for NGC 6522 in the *Gaia* DR2 database (Gaia Collaboration 2018). Since NGC 6522 is relatively far ($d_\odot \sim 7.7$ kpc), we decided to pay particular attention to avoiding

[2] Here, the term second-generation refers to groups of stars in globular clusters that display altered light-element abundances (C, N, O, Na, Al, and Mg).

[3] ASPCAP: The APOGEE Stellar Parameter and Chemical Abundances Pipeline.

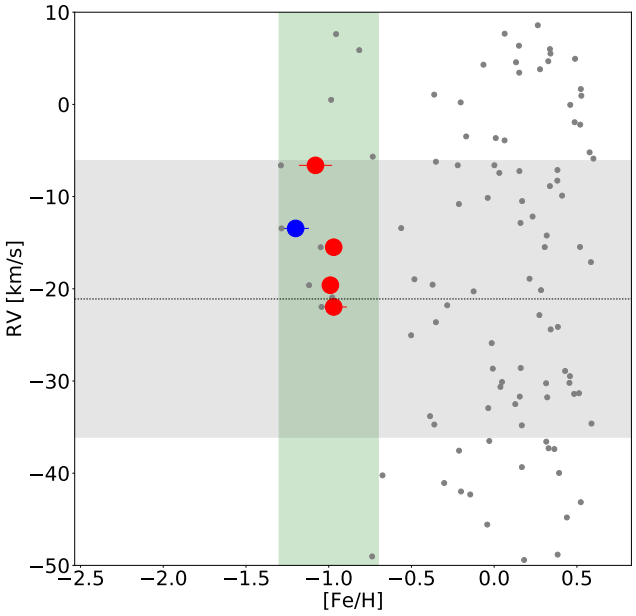

Fig. 1. TAPOGEE/DR14 radial velocity of the stars against their metallicity (gray dots). The red filled circles are the new highest-likelihood cluster members analyzed in this work, while the blue filled circle is the giant star analyzed in Schiavon et al. (2017a). The gray and green shadow region defines the upper and lower limits for the membership selection, and the black dotted line marks the radial velocity (-21.1 km s^{-1}) of NGC 6522 according to Harris (1996).

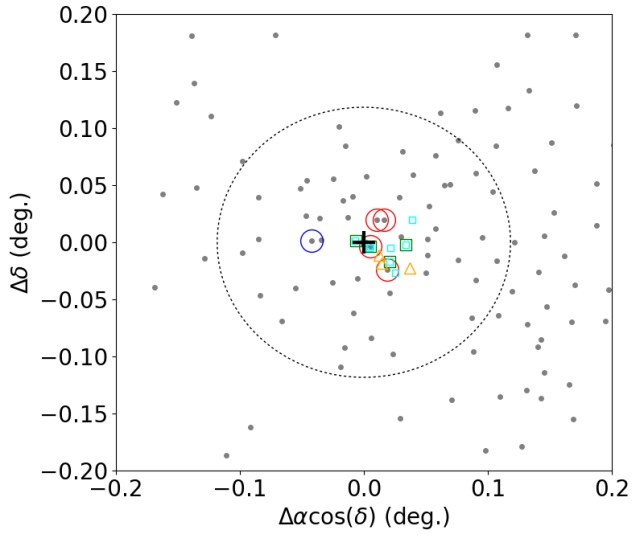

Fig. 2. Spatial distribution of targets in NGC 6522: Member candidates are highlighted with red open circles. The inner plus symbol is the center of the cluster and the black dotted line marks the tidal radius of the cluster: $r_t = 7.1^{+6.1}_{-3.7}$ arcmin. Field stars from the APOGEE survey located in the commissioning plate 4332, FIELD = BAADEWIN_001-04 are plotted using small gray symbols. The unfilled cyan squares, green squares, orange triangles, and the blue open circle show cluster members analyzed in Ness et al. (2014), Barbuy et al. (2014), Recio-Blanco et al. (2017), and Schiavon et al. (2017a), respectively.

contamination by data processing artifacts and/or spurious measurements. Therefore, we adopted the following conservative cuts on the columns of the *Gaia* DR2 `GAIA_SOURCE` catalog:

(1.) `ASTROMETRIC_GOF_AL` < 8. This cut ensures that the statistics astrometric model resulted in a good fit to the data.

(2.) `ASTROMETRIC_EXCESS_NOISE_SIG` ≤ 2. This criterion ensured that the selected stars were astrometrically well-behaved sources.

(3.) $-0.23 \leq$ `MEAN_VARPI_FACTOR_AL` ≤ 0.32 `AND` `VISIBILITY_PERIODS_USED` > 7. These cuts were used to exclude stars with parallaxes more vulnerable to errors.

(4.) $G < 19$ mag. This criterion minimized the chance of foreground contamination.

The final sample thus selected amounts to a total of 45 683 stars, which lie in a radius of 0.3° around the NGC 6522. Figure 3 shows the spatial distribution, proper motion distribution, and CMD of the *Gaia* DR2 stars labeled as members (black dots) of NGC 6522 as well as *Gaia* DR2 field stars and the newly identified second-generation stars (blue and red unfilled circles). To select *Gaia* DR2 stars as potential members, we adopt σ_μ as the total uncertainty in quadrature obtained from a 2D Gaussian fit. For this purpose, a 2D Gaussian smoothing routine was applied in proper motion space for stars with $G < 19$ mag within the cluster tidal radius. A 2D Gaussian was fitted to this sample and membership probabilities were assigned. With this procedure, we found $\mu_\alpha^{2D} \pm \sigma_\alpha = 2.539 \pm 0.510$ mas yr^{-1}, $\mu_\delta^{2D} \pm \sigma_\delta = -6.399 \pm 0.449$ mas yr^{-1}, and $\sigma_\mu = 0.608$ mas yr^{-1}. Our results also agree remarkably well with the more recent measurements of PMs for NGC 6522; for example: $\mu_\alpha = 2.618 \pm 0.072$ mas yr^{-1}, and $\mu_\delta = -6.431 \pm 0.071$ from Vasiliev (2019). A star was considered to be a GC member if its proper motion was found to differ from that of NGC 6522 by not by more than $3\sigma_\mu$. One can see that the newly identified N-rich stars from the APOGEE survey are distributed inside the tidal radius of the cluster and the proper motions of those stars match the nominal proper motion of NGC 6522. The *Gaia* DR2 CMD contains the stars with the highest [N/Fe] in our sample along the red giant branch (RGB) of NGC 6522. Based on the *Gaia* DR2 (μ_α,μ_δ) space, we rule out other possible cluster candidates in our APOGEE sample, which are highlighted by green unfilled symbols in Fig. 3 and lie in the green shadow region (gray dots) in Fig. 1.

The positions on the CMD of the likely candidate members of NGC 6522 analyzed in this paper are shown in Fig. 4. One can immediately notice that the selected stars from the APOGEE survey lie in the upper part of the RGB indicated by red and blue filled symbols, and occupy the same locus as other potential stellar cluster candidates inside the half-light radius $r_{hl} = 0.56^{+0.41}_{-0.12}$ arcmin – see Cohen et al. (2017) for details about VVV+2MASS (Skrutskie et al. 2006; Minniti et al. 2010) CMDs of this cluster. The faintest star in these diagrams corresponds to the star 2M18033660−3002164 ($K_{s\,VVV} = 12.272$ and $G = 15.322$), while 2M18032356−3001588 ($K_{s\,VVV} = 9.157$ and $G = 12.920$) is the brightest star as listed in Table 1.

4. Light-element abundances in NGC 6522

In this work, we employed the Brussels Automatic Stellar Parameter (BACCHUS)[4] code (see Masseron et al. 2016;

[4] The previous (DR12) and current (DR13/14) version of ASPCAP does not determine the abundances of the neutron-capture elements Ce and Nd, but the recent characterization (e.g., oscillator strenghts) of the H-band Nd II and Ce II lines (Hasselquist et al. 2016; Cunha et al. 2017) permits, in principle, the derivation of their abundances using a spectral synthesis code like BACCHUS (see text for more details). The synthetic spectra were based on 1D LTE model atmospheres calculated with MARCS (Gustafsson et al. 2008) using the solar abundance table from Asplund et al. (2005), except for Ce, for which we adopted the abundance table from Grevesse et al. (2015). For consistency (among other reasons), we re-derived all abundances with BACCHUS.

Table 1. G, G_{BP}, G_{RP}, and J, H, Ks VVV+2MASS magnitudes and kinematics information for the five giant stars analyzed in this work.

APOGEE ID	G	G_{BP}	G_{RP}	J_{2MASS}	H_{2MASS}	Ks_{2MASS}	J_{VVV}	H_{VVV}	Ks_{VVV}	V_{helio} (km s^{-1})	$V_{scatter}$ (km s^{-1})	N_{visits}	S/N (pixel^{-1})
2M18032356−3001588	12.920	14.109	11.847	10.153 ± 0.022	9.174 ± 0.025	8.936 ± 0.023	10.171 ± 0.001	9.381 ± 0.001	9.157 ± 0.001	−13.45 ± 0.01	2.59	3	308.8
2M18034052−3003281	14.789	15.679	13.781	12.109 ± 0.025	11.298 ± 0.027	11.113 ± 0.027	12.291 ± 0.002	11.715 ± 0.002	11.406 ± 0.002	−21.97 ± 0.02	0.32	7	71.1
2M18033965−3000521	14.661	15.484	13.618	11.836 ± 0.034	11.104 ± 0.035	10.897 ± 0.034	12.198 ± 0.002	...	11.329±0.002	−19.61 ± 0.03	0.11	4	57.6
2M18033819−3000515	13.618	14.569	12.577	10.996 ± 0.028	10.106 ± 0.026	9.907 ± 0.03	11.195 ± 0.001	11.201 ± 0.001	10.030 ± 0.001	−15.49 ± 0.01	0.05	3	190.6
2M18033660−3002164	15.322	15.818	14.144	13.006 ± 0.045	11.803	11.574	13.022 ± 0.004	12.443 ± 0.004	12.272 ± 0.005	−6.61 ± 0.06	0.27	7	61.6

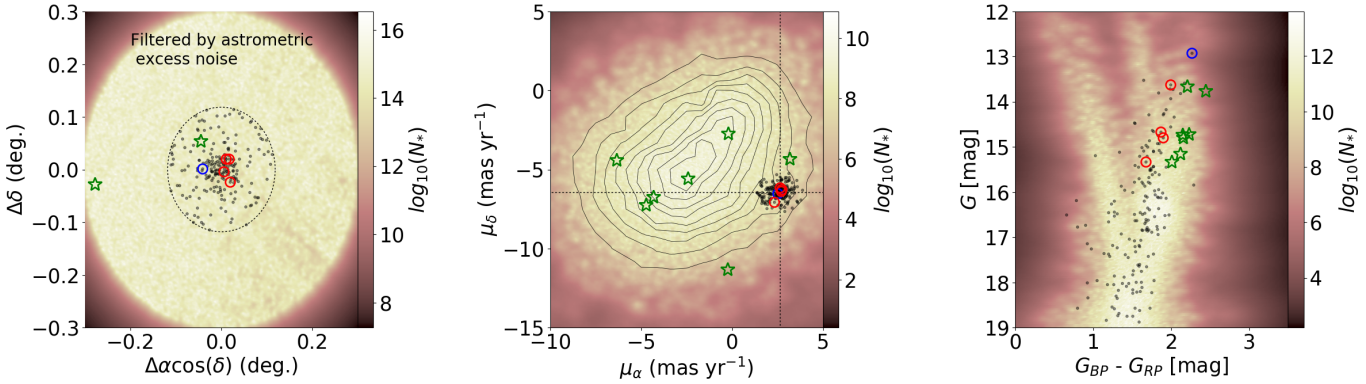

Fig. 3. Kernel density estimate (KDE) smoothed distribution (*left*), proper motion distribution (*middle*), and CMD (*right*) of *Gaia* DR2 stars toward the NGC 6522 field. *Leftmost panel*: position of the newly detected member cluster candidates (red unfilled circles), the blue unfilled circle represents the star previously reported in Schiavon et al. (2017a), the green unfilled stars show the position of the field stars contained within the green shadow region as illustrated in Fig. 1, the black dots represent the *Gaia* DR2 stars inside the tidal radius of the cluster and whose proper motions match with the nominal proper motion of NGC 6522 within $3\sigma_\mu$, and the black dotted circle marks the size of the tidal radius of the cluster. The middle plot shows (μ_α,μ_δ) distribution and the black dotted lines show the nominal proper motion of NGC 6522. The rightmost plot shows the *Gaia* DR2 CMD of each star.

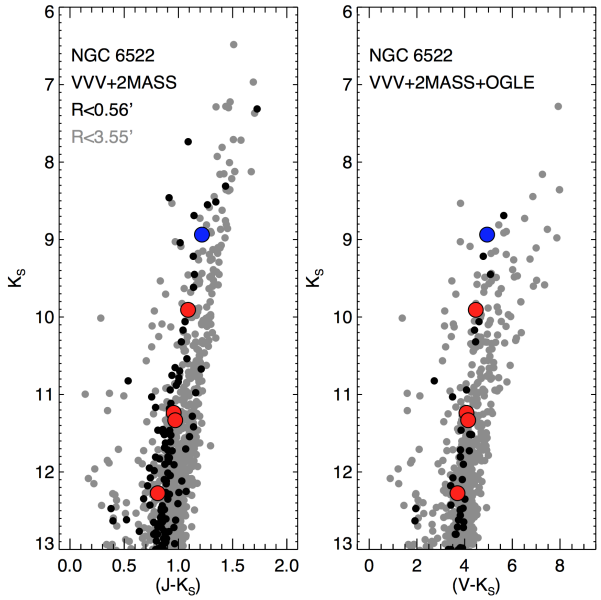

Fig. 4. Color–magnitude diagram of (VVV+2MASS K_s, $J - K_s$) and VVV+2MASS K_s+OGLE from Cohen et al. (2017), illustrating the positions of all the stars inside half the tidal radius (gray dots), and all the stars inside the half-light radius (black dots), $r_{hl} = 0.56^{+0.41}_{-0.12}$ arcmin, with the position of the APOGEE spectroscopic targets superimposed. The symbols are the same as in Fig. 1.

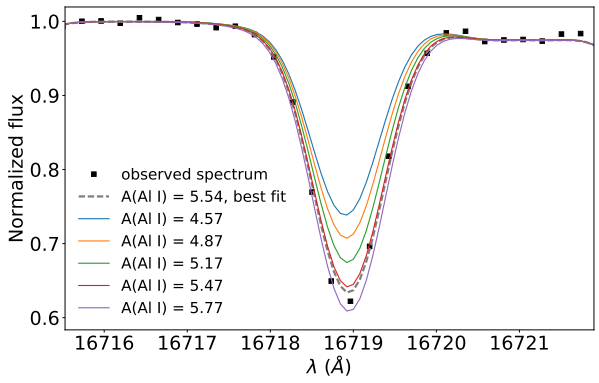

Fig. 5. High-resolution H-band observed spectrum of 2M18034052−3003281 (filled squares) in the 16716–16721 Å (Al I line) region. Superimposed are MARCS/BACCHUS synthetic spectra. All spectra are expressed in air wavelengths.

Hawkins et al. 2016) to derive chemical abundances for up to eight chemical elements that are typical indicators of stars with "polluted chemistry" in GCs (C, N, O, Al, Mg, and Si: see, e.g., Tang et al. 2017; Schiavon et al. 2017a).

All the chemical species were first visually inspected line-by-line and rejected if they were found to be problematic, such as those heavily blended by telluric features. We note that in contrast to ASPCAP pipeline (which employs KURUCZ atmospheric models, e.g., see García Pérez et al. 2016), we provide a line-by-line analysis based on MARCS model atmosphere grid. Table 3 lists the wavelength regions used to obtain the individual abundances, while Fig. 5 plots an example of the best fits obtained using MARCS/BACCHUS synthetic spectra around the Al I line, λ_{air} = 16718.957 Å. BACCHUS software provides four different abundance determinations: (i) line-profile fitting; (ii) core line intensity comparison; (iii) global goodness-of-fit estimate (χ^2); and (iv) equivalent width comparison; and each diagnostic yields validation flags. Based on these flags, a

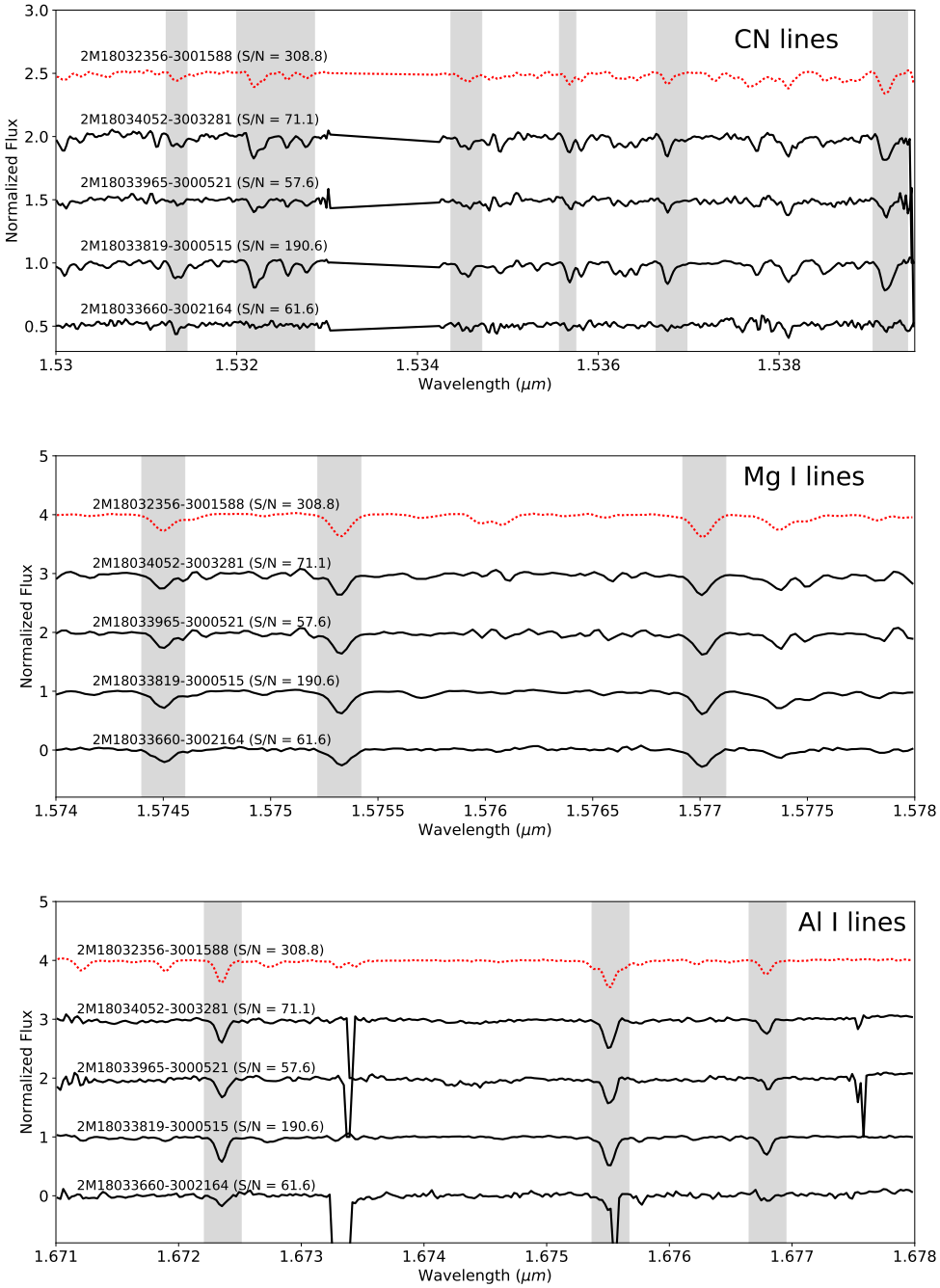

Fig. 6. APOGEE combined spectra of the analyzed stars in a narrow spectral window, covering the regions (gray shadow) around the CN features (*top panel*), Mg I lines (*middle panel*), and Al I lines (*bottom panel*) used to estimate N, Mg, and Al abundances. A quick comparison between the stars identified in this work and the APOGEE star (red line) with second-generation abundance patterns identified in a previous paper (Schiavon et al. 2017a) indicates that we would be able to detect very large N and Al enhancements. (Alonso-García et al. 2012).

decision tree then rejects the line or accepts it, keeping the best-fit abundance (see, e.g., Hawkins et al. 2016). Following the suggestion by Hawkins et al. (2016), we subsequently adopt the χ^2 diagnostic as the abundance, which is the most robust.

In Fig. 6, we plot several portions of the observed APOGEE spectra, showing examples of the windows used in our chemical analysis to extract the N, Al, and Mg abundances from the CN lines, Al I, and Mg I spectral features, respectively. The $^{12}C^{14}N$ and Al I lines are strong for the $T_{\rm eff}$, log g, and metallicity range of our sample stars, already indicating that they are enhanced in N and Al. The only exception, as expected, is the hottest star in our sample (2M18033660−3002164), which displays much weaker CN, Al I, and Mg I spectral lines in its relatively low-S/N spectrum, making their abundances more uncertain (in particular for N; see e.g., Mészáros et al. 2015).

To avoid any spurious results, we rejected the two sodium lines at 1.6373 μm and 1.6388 μm, as they are very weak in the typical $T_{\rm eff}$, log g, and metallicity range of our sample, leading to unreliable [Na/Fe] abundances. In addition, lines such as Nd II, Na I, Cr I, Mn I, Ni I, and other chemical species were rejected, as they were found to be weak and heavily blended by other features, which can alter the abundances.

For each star, the abundances are then derived by means of a line-by-line analysis using the BACCHUS pipeline and MARCS model atmospheres (Gustafsson et al. 2008). The line list adopted in this work is the version linelist.20150714, which was used for the DR14 results (Abolfathi et al. 2018), and includes both atomic and molecular species. For a more detailed description of these lines, we refer the reader to a forthcoming paper (Holtzman et al. in preparation).

Table 2. Mean abundance as derived from BACCHUS for elements which have more than one line.

APOGEE ID	2M18032356−3001588	2M18033819−3000515	2M18033965-3000521	2M18034052−3003281	2M18033660−3002164
$T_{\rm eff}$ (K)	3977.2	4378.1	4555.8	4492.3	5021.1
log g (dex)	0.50	1.09	1.35	1.26	1.99
ξ_t (km s^{-1})	2.46	2.67	2.43	1.92	1.37
[Fe/H]	−1.20	−0.97	−0.99	−0.97	−1.08
[C/Fe]	−0.48	−0.33	−0.29	−0.24	...
[N/Fe]	1.29	1.30	1.03	1.20	1.13
[O/Fe]	0.39	0.30	0.29	0.35	...
[Al/Fe]	0.38	0.77	0.39	0.93	0.39
[Mg/Fe]	0.16	0.04	0.05	0.05	0.33
[Si/Fe]	0.28	0.17	0.18	0.37	0.51
[Ce/Fe]	0.09	0.23	...	...	...

Notes. The Solar reference abundances are from Asplund et al. (2005), except for Ce, which is taken from Grevesse et al. (2015).

For each sample star, we need $T_{\rm eff}$ and log g as input parameters in BACCHUS. Thus, we decided to use the DR14 ASPCAP uncalibrated effective temperature ($T_{\rm eff}^{\rm raw}$)[5] that comes from the best ASPCAP global fit to the observed spectra as well as independent surface gravities from PARSEC (Bressan et al. 2012) isochrones (chosen to be 12 Gyr). With fixed $T_{\rm eff}$ and log g, the first step consists of determining the metallicity, the ξ_t parameter, and the convolution parameter, that is, the metallicity provided is the average abundance of selected Fe lines, and the $\xi_{\rm t}$ is obtained by minimizing the trend of Fe abundances against their reduced equivalent width, while the convolution parameter stands for the total effect of the instrument resolution, the macroturbulence, and $v \sin i$ on the line broadening (e.g., Hawkins et al. 2016). In addition, we adopted the C, N, and O abundances that satisfy the fitting of all molecular lines consistently; that is, we first derive O abundances from OH, then derive C from CO, and then N from CN lines and the CNO abundances are derived several times to minimize the OH, CO, and CN dependences (see e.g., Smith et al. 2013; Souto et al. 2016). The mean abundances determined with these input atmospheric parameters and the BACCHUS pipeline are listed in Table 2.

In Table 3, we indicate the typical uncertainty of our abundance determinations, that is, the uncertainty in each of the atmospheric parameters. The final uncertainty for each element was calculated as the root squared sum of the individual uncertainties due to the errors in each atmospheric parameter under the assumption that these individual uncertainties are independent. The reported uncertainty for each chemical species is: $\sigma_{\rm total} = \sqrt{\sigma^2_{\rm [X/H],T_{eff}} + \sigma^2_{\rm [X/H],logg} + \sigma^2_{\rm [X/H],\xi_t} + \sigma^2_{\rm mean}}$; where $\sigma^2_{\rm mean}$ is calculated using the standard deviation from the different abundances of the different lines for each element, while $\sigma^2_{\rm [X/H],T_{eff}}$, $\sigma^2_{\rm [X/H],logg}$, and $\sigma^2_{\rm [X/H],\xi_t}$ are derived for each chemical species while varying $T_{\rm eff}$ by ±100 K, log g by ±0.3 dex, and $\epsilon_{\rm t}$ by ±0.05 km s^{-1}. These values were chosen as they represent the typical uncertainty in the atmospheric parameters for our sample.

It is important to note that our line-by-line abundances provides evidence that the new NGC 6522 members reported here are enriched in N and Al, probing the second-generation nature of these stars.

[5] In contrast to Mészáros et al. (2015), we chose not to estimate the $T_{\rm eff}$ values from any empirical color–temperature relation; this is highly uncertain due to the relatively high NGC 6522 reddening, $E(J-K) \sim 0.25$ (see e.g., Schultheis et al. 2017).

5. Cerium abundances in NGC 6522

As mentioned above, the two neutron-capture elements Ce and Nd have been detected in APOGEE spectra until now (via their Nd II and Ce II H-band absorption lines; Hasselquist et al. 2016; Cunha et al. 2017), providing a unique opportunity to determine the elemental abundances of these elements from H-band spectra. Unfortunately, the ten Nd II lines between 15284.5 and 16634.7 Å (see Table 3 in Hasselquist et al. 2016) are too weak (and/or heavily affected by telluric features) in the APOGEE spectra of our sample stars, and are therefore not useful for the Nd abundance determination. However, four strong and clean Ce II lines (see Table 3) are clearly detected in two sample stars (2M18032356−3001588 and 2M18033819−3000515), allowing us to estimate their Ce abundances.

The star 2M18032356−3001588 was previously analyzed by (Schiavon et al. 2017a) and its Ce abundance ([Ce/Fe] = +0.10 dex) was provided by Cunha et al. (2017). We measure a BACCHUS-based mean Ce abundance of [Ce/Fe] = +0.09 ± 0.04, which is in excellent agreement with the one reported by Cunha et al. (2017), while our C, Fe, Al, and Mg abundances agree within ∼0.1 dex with the DR12 abundances reported by (Schiavon et al. 2017a); the only exception is N, for which we find a higher N abundance (by 0.25 dex; [N/Fe] = 1.29). Thus, 2M18032356−3001588 displays a chemical composition somehow intermediate between the first generation (FG) and second-generation stars in the Mg–Al plane as compared to other GCs at similar metallicity (see Fig. 7, left panel).

The star 2M18033819−3000515 also shows a N-enrichment very similar to that of 2M18032356−3001588. Contrary to 2M18032356−3001588, the star 2M18033819−3000515 displays a mildly enhanced Ce abundance of [Ce/Fe] = +0.23 ± 0.03, which is accompanied by a higher Al content (and lower Mg) which is consistent with a second-generation nature.

For 2M18033965−3000521, 2M18034052−3003281, and 2M18033660−3002164, the Ce II absorption lines are heavily affected by telluric features, are too weak to be derived, and were not well reproduced by the synthesis. Therefore, we do not provide the [Ce/Fe] abundance ratios for these stars.

6. Discussion

Two of the stars analyzed in the present sample (2M18033819−3000515 and 2M18034052−3003281) show high Al abundances ([Al/Fe] > + 0.77), and are potentially associated with a

Table 3. Typical uncertainty of the abundance determinations from our present measurements.

APOGEE-ID	X	$\sigma_{[X/H],T_{eff}}$	$\sigma_{[X/H],\log g}$	$\sigma_{[X/H],\xi_t}$	σ_{mean}	σ_{total}
2M18032356−3001588	Fe	0.055	0.033	0.041	0.050	0.091
2M18032356−3001588	C	0.038	0.132	0.081	0.030	0.162
2M18032356−3001588	N	0.172	0.135	0.122	0.060	0.257
2M18032356−3001588	O	0.141	0.075	0.076	0.070	0.190
2M18032356−3001588	Mg	0.092	0.097	0.071	0.050	0.159
2M18032356−3001588	Al	0.075	0.053	0.067	0.010	0.114
2M18032356−3001588	Si	0.022	0.017	0.021	0.100	0.106
2M18032356−3001588	Ce	0.044	0.072	0.039	0.040	0.101
2M18034052−3003281	Fe	0.054	0.035	0.024	0.080	0.105
2M18034052−3003281	C	0.084	0.121	0.040	0.020	0.154
2M18034052−3003281	N	0.190	0.151	0.039	0.100	0.265
2M18034052−3003281	O	0.146	0.049	0.017	0.020	0.156
2M18034052−3003281	Mg	0.060	0.066	0.044	0.060	0.116
2M18034052−3003281	Al	0.118	0.098	0.031	0.060	0.168
2M18034052−3003281	Si	0.033	0.025	0.014	0.090	0.100
2M18034052−3003281	Ce	…	…	…	…	…
2M18033965−3000521	Fe	0.032	0.041	0.008	0.040	0.066
2M18033965−3000521	C	0.071	0.092	0.116	0.040	0.169
2M18033965−3000521	N	0.121	0.071	0.149	0.050	0.211
2M18033965−3000521	O	0.121	0.053	0.027	0.020	0.136
2M18033965−3000521	Mg	0.068	0.037	0.019	0.050	0.094
2M18033965−3000521	Al	0.099	0.041	0.021	0.02	0.111
2M18033965−3000521	Si	0.032	0.067	0.024	0.06	0.098
2M18033965−3000521	Ce	…	…	…	…	
2M18033819−3000515	Fe	0.061	0.092	0.011	0.050	0.122
2M18033819−3000515	C	0.020	0.133	0.017	0.040	0.141
2M18033819−3000515	N	0.148	0.234	0.010	0.050	0.282
2M18033819−3000515	O	0.149	0.025	0.003	0.070	0.166
2M18033819−3000515	Mg	0.128	0.201	0.034	0.080	0.254
2M18033819−3000515	Al	0.244	0.277	0.037	0.070	0.378
2M18033819−3000515	Si	0.163	0.214	0.046	0.080	0.284
2M18033819−3000515	Ce	0.045	0.143	0.004	0.030	0.153
2M18033660−3002164	Fe	0.049	0.018	0.037	0.100	0.119
2M18033660−3002164	C	…	…	…	…	…
2M18033660−3002164	N	0.247	0.103	0.059	0.130	0.303
2M18033660−3002164	O	…	…	…	…	…
2M18033660−3002164	Mg	0.071	0.077	0.044	0.150	0.188
2M18033660−3002164	Al	0.065	0.033	0.057	…	0.093
2M18033660−3002164	Si	0.043	0.018	0.025	0.290	0.295
2M18033660−3002164	Ce	…	…	…	…	…

second stellar generation. This is also corroborated by the high N ([N/Fe] > + 1.0), indicating a clear correlation between these two elements. This is in good agreement with the self-enrichment scenario where the origin of the SG chemical pattern is attributed to the pollution with gas reprocessed by proton-capture nucleosynthesis (see Mészáros et al. 2015). The other three stars in the sample (2M18032356−3001588, 2M18033965−3000521, and 2M18033660−3002164) exhibit lower Al enhancement (∼+0.4 dex) with respect to the solar-scaled Al-abundance, but are clearly highly N enhanced ([N/Fe] > + 1.0), occupy the locus dominated by second-generation globular cluster stars at similar metallicity, and are separated relatively cleanly in the [N/Fe]–[Fe/H] plane; see Fig. 7.

We caution on the accuracy of [Al/Fe] for 2M18033660−3002164, whose Al I line in λ^{air} = 16710 Å is weaker; while it has a high N abundance, we warn that these lines are not reliable. For $^{12}C^{16}O$ and ^{16}OH, the lines are weak and heavily blended by telluric features. At this time, we cannot guarantee the quality of the [C/Fe] and [O/Fe] abundances for 2M18033660−3002164, but this is not the case for $^{12}C^{14}N$ and therefore the [N/Fe] abundance ratios have been derived by fixing A(C) and A(O) using the reported [O/Fe] and [C/Fe] from Chiappini et al. (2011); star B-107 (2M18033660−3002164) in that work.

Any conclusion given on the basis of the Mg abundances is less trivial. The small size of the APOGEE sample discussed here limits the possibility of clearly identifying stars of the FG. This particularly affects any conclusion on the presence or not of Mg depletion in this cluster based solely on APOGEE data. In clusters of similar metallicity, the Mg variation between FG and SG members is generally smaller (≤+0.2 dex, see, e.g., Mészáros et al. 2015) than what is observed in Al and N. More caution must be taken when considering that such Mg variation is comparable with the abundance uncertainties. Nevertheless, the APOGEE data suggest the presence of a Mg–Al anticorrelation. This Mg–Al anticorrelation has also been observed by (Ness et al. 2014), where abundances for a larger sample of stars (8) have been measured. From Fig. 7 however the Mg measurements from Ness et al. seem to be systematically higher than those of the present APOGEE sample and the Recio-Blanco et al. (2017) sample. This is also confirmed by Barbuy et al. (2014), who found [Mg/Fe] to be systematically higher (∼ + 0.2 dex) for four stars in common with the Ness et al. (2014) sample. A larger stellar sample, analyzed in a homogeneous fashion, with more accurate abundances, is needed to further confirm the presence of a possible Mg spread between FG and SG stars. This is also what is needed in order to directly compare these observations with any GC formation or evolution scenario proposed so far to explain the origin of the MPs (see, e.g., Bastian & Lardo 2018, for a general review). Most of the stars in our final dataset lie in a group with super-solar [N/Fe] and [Al/Fe], and clearly extend beyond of the typical chemical abundances observed in Milky Way field stars.

The [O/Fe] abundance ratios listed in Table 2 are generally higher compared with APOGEE-DR14/ASPCAP results by ∼+0.15 dex, showing that [O/Fe] abundance ratios are particularly sensitive to log g. As the abundances of C and O affect CN lines (see Schiavon et al. 2017a), it can seen in Table 2 that the variations in [O/Fe] do not significantly affect the [N/Fe] abundance ratios in our sample, which turn out to be nitrogen rich, with remarkably stronger CN lines with nonenhanced carbon abundances ([C/Fe] ≲ +0.15). In other words, these stars exhibit clear N enhancements, even when [O/Fe] is slightly sensitive to log g.

As mentioned above, the newly identified stellar members of NGC 6522 display enhancements in [Al/Fe], suggesting that NGC 6522 exhibits large scatter in its Al abundance ratios. Combining our results with the abundance analyses from Ness et al. (2014) and Recio-Blanco et al. (2017), we infer Al variations of Δ[Al/Fe] ∼ 1 dex. Such Al enhancements provide an indication that MPs with distinctive chemistries are present in NGC 6522, and that the MgAl cycles have been activated. Figure 7 clearly shows the Mg–Al anti-correlation in our sample, and the [Mg/Fe] abundances show a much smaller variation (Δ[Mg/Fe] ≲ +0.2 dex) in our MARCS/BACCHUS determinations. However, the combined datasets show that Mg exhibits significantly larger scatter than any implicit systematic error. This comparison allows us to confirm the conversion of Mg into Al during the MgAl cycles, which is present in NGC 6522. The summed abundance A(Mg+Al) is expected to be constant as a function of T_{eff} when material is completely processed through the MgAl cycle, and that is what our results show in Fig. 8. This finding is a clear confirmation of the results reported in our previous work (see Schiavon et al. 2017a; Recio-Blanco et al. 2017).

Concerning silicon, we found over-abundances of [Si/Fe] ratios on the order of ∼+0.3, which is similar to APOGEE-DR14/ASPCAP values, with a reasonably small scatter, within our measurement errors. So far, our abundance values fall into acceptable ranges with the literature on abundance

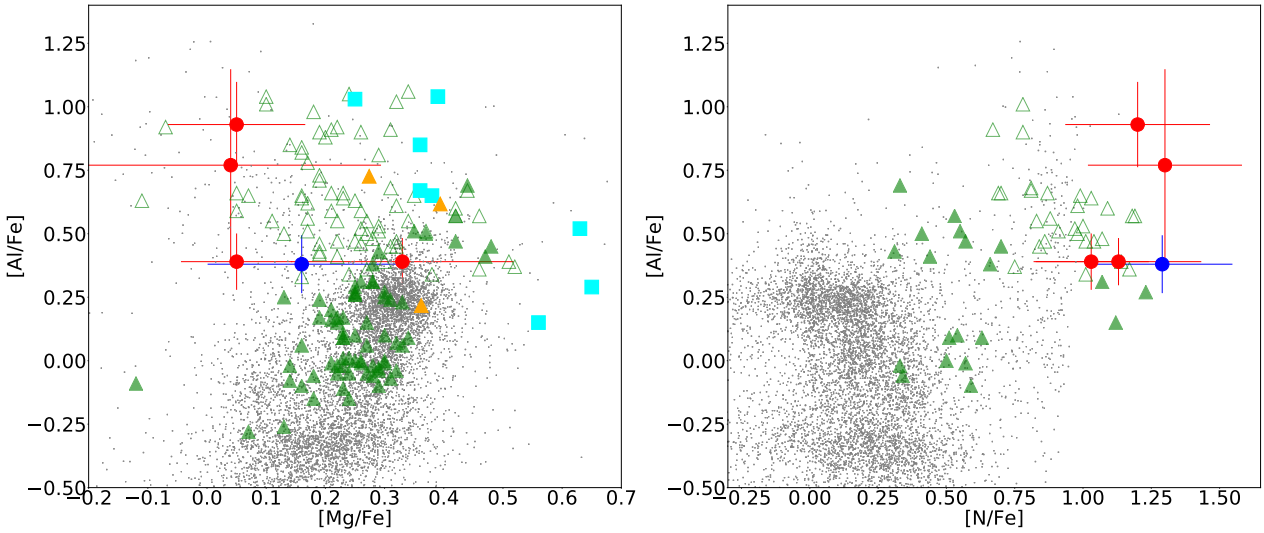

Fig. 7. Behavior of the average [Al/Fe], [Mg/Fe], and [N/Fe] abundance ratios of our synthesis analysis (red and blue filled symbols) compared with DR14 abundances from field stars (gray dots), and overplotted with APOGEE DR14 determinations for the first (green filled triangles) and second populations (green empty triangles) in GCs M 5, M 71, and M 107 (Mészáros et al. 2015). Orange triangles and cyan squares are very likely members of NGC 6522 from the *Gaia*-ESO survey; Recio-Blanco et al. (2017) and Ness et al. (2014), respectively.

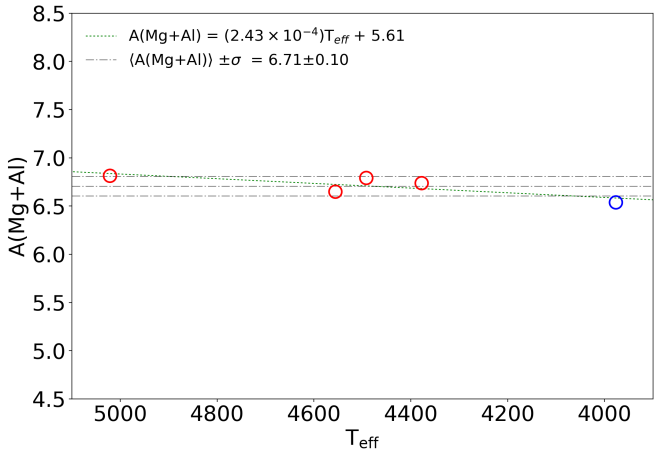

Fig. 8. Combined abundance of A(Mg+Al) as a function of effective temperature ($T_{\rm eff}$). The symbols have the same meaning as those in Fig. 2.

studies in globular cluster stars (e.g., see Carretta et al. 2012; Mészáros et al. 2015; Recio-Blanco et al. 2017). We find that the Si–Al correlation is also weak in our data. This could be interpreted as evidence for Si leaking from the Mg–Al cycle (for discussion and references, see, e.g., Tang et al. 2017), that is, one would expect the Si enhancement to be correlated with Al in metal-poor globular clusters where the AGB stars burn slightly hotter or in high-mass clusters where the chemical enrichment is more efficient (see Carretta et al. 2009a; Mészáros et al. 2015).

Radial velocity variation: The stars 2M18033819−3000515, 2M18033965−3000521, 2M18034052−3003281, and 2M18033660−3002164 were visited 3, 4, 7, and 7 times, respectively, by the APOGEE survey. This allow us to identify any significant variation in their radial velocities, and thereby add empirical constraints to the origin of the observed N and Al over-abundances. Given that the typical variation in radial velocity measured for these stars is of the order of $V_{\rm scatter} < 0.4\,{\rm km\,s^{-1}}$ (see Nidever et al. 2015), this rules out the binary mass-transfer hypothesis (see Schiavon et al. 2017b) as a possible source of pollution.

It is important to note that the derived [Ce/Fe] ratios are compatible with previous studies that found low s-process abundances, such as for example Ness et al. (2014). Our results support the hypothesis that the *s*-process rich material in NGC6522 could have been formed via pollution of pristine gas from a former population of massive AGB stars (e.g., Ventura et al. 2016; Dell'Agli et al. 2018; Fishlock et al. 2014) and, on the other hand, do not support a scenario in which the spinstars are the main polluters.

Finally, Fernández-Trincado et al. (2017b,a, 2019d) recently discovered a new N- and Al-rich ([N/Fe] and [Al/Fe] ratios around ∼+1.0 dex) population of stars on very eccentric orbits ($e > 0.65$) in the Milky Way field (towards the bulge, the disk, and the halo), passing through the inner regions of the Milky Way bulge. Whether or not globular clusters at similar metallicities are able to kick out stars with similar chemical behavior, as seen in the innermost regions of NGC 6522, it is not impossible that a few field stars with similar chemistry patterns (Schiavon et al. 2017b; Fernández-Trincado et al. 2017b, 2019a,b,c,d, for instance) could have been ejected from these bulge cluster environments with a relative velocity greater that the escape velocity of the GCs, particularly being ejected from some scenarios involving binary systems or black hole interactions (see, e.g., Hut 1983; Heggie et al. 1996; Pichardo et al. 2012; Fernández-Trincado et al. 2013, 2015b,a, 2016b), or due to simple tidal forces (Küpper et al. 2012; Lane et al. 2012). In turn, these could be capable of exceeding the escape velocity at the radius of the bulge (∼650 km s^{-1}), meaning that we would expect a few of the N-rich stars with enhanced Al abundances ([Al/Fe] $\gtrsim$ +0.6) not to be part of the Milky Way bulge, and would not be surprised to see eccentric orbits, as was the case recently. More accurate distances and proper motions are needed to confirm this hypothesis.

7. Concluding remarks

We used an independent pipeline called BACCHUS (see Masseron et al. 2016; Hawkins et al. 2016), an updated line list, and careful line selection to explore the chemical abundance

patterns of five potential members of the globular cluster NGC 6522.

The distinctive chemical patterns characterizing MPs, especially simultaneous enrichment in nitrogen and aluminium with low carbon-abundance ratios ([C/Fe] < +0.15), have been measured in our sample, and have been used to confirm the presence of MPs in NGC 6522.

The main results of our chemical abundance analysis from high-resolution APOGEE spectra in NGC 6522 potential members can be summarized as follows.

- We report the identification of three new potential stellar members (2M18033819−3000515, 2M18033965−3000521, and 2M18034052−3003281) of NGC 6522 in the APOGEE survey (Majewski et al. 2017). The spectra analyzed in this work have $S/N > 50$, exhibiting very similar line strengths (namely CN bands, Al I and Mg I lines) to that of 2M18032356−3001588 (see Schiavon et al. 2017b), making them ideal for line-by-line spectrum synthesis calculations of selected clean features. These spectral properties suggest that the stars of this group share a common formation history and spatial relationship on the sky, and are therefore gravitationally bound to NGC 6522.
- We measured significant N and Al over-abundances, with carbon depletion in NGC 6522 members, suggesting that the distinctive chemical patterns characterizing MPs is present within NGC 6522, reinforcing recent claims in the literature (Schiavon et al. 2017a; Recio-Blanco et al. 2017; Kerber et al. 2018).
- Lastly, we do not find any enhancement in heavy elements measured from APOGEE spectra (Ce II). We measured only mildly enhanced [Ce/Fe] < 0.25 abundance ratios, in agreement with recent optical studies, which goes against previous observational evidence for the chemical signatures of rapidly rotating Population III stars ("spinstars") in NGC 6522. Such low *s*-process abundances could still be consistent with other intra-cluster medium polluters such as massive AGB stars.

Acknowledgements. We would like to thank the referee for insightful comments which helped to improve this work. J.G.F-T, P.L-P, and J.A-G were supported by MINEDUC-UA project, code ANT 1855. J.G.F-T also acknowledges financial support from the FONDECYT No. 3180210 and the ChETEC COST Action (CA16117), supported by COST (European Cooperation in Science and Technology). D.G. gratefully acknowledges support from the Chilean Centro de Excelencia en Astrofísica y Tecnologías Afines (CATA) BASAL grant AFB-170002. D.G. also acknowledges financial support from the Dirección de Investigación y Desarrollo de la Universidad de La Serena through the Programa de Incentivo a la Investigación de Académicos (PIA-DIDULS). S.V gratefully acknowledges the support provided by Fondecyt reg. n. 1170518. Szabolcs Mészáros has been supported by the Premium Postdoctoral Research Program of the Hungarian Academy of Sciences, and by the Hungarian NKFI Grants K-119517 of the Hungarian National Research, Development and Innovation Office. R.E.M. acknowledges project fondecyt 1190621. D.M. and J.A-G. are supported also by FONDECYT No. 1170121 and 11150916 respectively, and by the Ministry of Economy, Development, and Tourism's Millennium Science Initiative through grant IC120009, awarded to the Millennium Institute of Astrophysics (MAS). DAGH, OZ, FDA, and TM acknowledge support from the State Research Agency (AEI) of the Spanish Ministry of Science, Innovation and Universities (MCIU) and the European Regional Development Fund (FEDER) under grant AYA2017-88254-P. T.C.B. acknowledges partial support from grant PHY 14-30152: Physics Frontier Center/JINA Center for the Evolution of the Elements (JINA-CEE), awarded by the US National Science Foundation. BACCHUS have been executed on computers from the Institute of Astronomy and Planetary Sciences at Universidad de Atacama. This work has made use of results from the European Space Agency (ESA) space mission *Gaia*, the data from which were processed by the *Gaia* Data Processing and Analysis Consortium (DPAC). Funding for the DPAC has been provided by national institutions, in particular the institutions participating in the *Gaia* Multilateral Agreement. The *Gaia* mission website is http://www.cosmos.esa.int/gaia. Funding for the Sloan Digital Sky Survey IV has been provided by the Alfred P. Sloan Foundation, the U.S. Department of Energy Office of Science, and the Participating Institutions. SDSS-IV acknowledges support and resources from the Center for High-Performance Computing at the University of Utah. The SDSS web site is www.sdss.org. SDSS-IV is managed by the Astrophysical Research Consortium for the Participating Institutions of the SDSS Collaboration including the Brazilian Participation Group, the Carnegie Institution for Science, Carnegie Mellon University, the Chilean Participation Group, the French Participation Group, Harvard-Smithsonian Center for Astrophysics, Instituto de Astrofìsica de Canarias, The Johns Hopkins University, Kavli Institute for the Physics and Mathematics of the Universe (IPMU)/University of Tokyo, Lawrence Berkeley National Laboratory, Leibniz Institut für Astrophysik Potsdam (AIP), Max-Planck-Institut für Astronomie (MPIA Heidelberg), Max-Planck-Institut für Astrophysik (MPA Garching), Max-Planck-Institut für Extraterrestrische Physik (MPE), National Astronomical Observatory of China, New Mexico State University, New York University, University of Dame, Observatório Nacional / MCTI, The Ohio State University, Pennsylvania State University, Shanghai Astronomical Observatory, United Kingdom Participation Group, Universidad Nacional Autónoma de México, University of Arizona, University of Colorado Boulder, University of Oxford, University of Portsmouth, University of Utah, University of Virginia, University of Washington, University of Wisconsin, Vanderbilt University, and Yale University.

References

Abolfathi, B., Aguado, D. S., Aguilar, G., et al. 2018, ApJS, 235, 42
Alam, S., Albareti, F. D., Allende Prieto, C., et al. 2015, ApJS, 219, 12
Albareti, F. D., Allende Prieto, C., Almeida, A., et al. 2017, ApJS, 233, 25
Alonso-García, J., Mateo, M., Sen, B., et al. 2012, AJ, 143, 70
Asplund, M., Grevesse, N., & Sauval, A. J. 2005, in Cosmic Abundances as Records of Stellar Evolution and Nucleosynthesis, eds. T. G. Barnes, III, & F. N. Bash, ASP Conf. Ser., 336, 25
Barbuy, B., Zoccali, M., Ortolani, S., et al. 2009, A&A, 507, 405
Barbuy, B., Chiappini, C., Cantelli, E., et al. 2014, A&A, 570, A76
Bastian, N., & Lardo, C. 2018, ARA&A, 56, 83
Bressan, A., Marigo, P., Girardi, L., et al. 2012, MNRAS, 427, 127
Carretta, E. 2016, ArXiv e-prints [arXiv:1611.04728]
Carretta, E., Bragaglia, A., Gratton, R. G., et al. 2007, A&A, 464, 967
Carretta, E., Bragaglia, A., Gratton, R., & Lucatello, S. 2009a, A&A, 505, 139
Carretta, E., Bragaglia, A., Gratton, R. G., et al. 2009b, A&A, 505, 117
Carretta, E., Bragaglia, A., Gratton, R., et al. 2010, ApJ, 712, L21
Carretta, E., Bragaglia, A., Gratton, R. G., Lucatello, S., & D'Orazi, V. 2012, ApJ, 750, L14
Chiappini, C., Frischknecht, U., Meynet, G., et al. 2011, Nature, 472, 454
Cohen, R. E., Moni Bidin, C., Mauro, F., Bonatto, C., & Geisler, D. 2017, MNRAS, 464, 1874
Cohen, R. E., Mauro, F., Alonso-García, J., et al. 2018, AJ, 156, 41
Cunha, K., Smith, V. V., Hasselquist, S., et al. 2017, ApJ, 844, 145
Dell'Agli, F., García-Hernández, D. A., Ventura, P., et al. 2018, MNRAS, 475, 3098
Eisenstein, D. J., Weinberg, D. H., Agol, E., et al. 2011, AJ, 142, 72
Fernández-Trincado, J. G., Vivas, A. K., Mateu, C. E., & Zinn, R. 2013, Mem. Soc. Astron. It., 84, 265
Fernández-Trincado, J. G., Robin, A. C., Vieira, K., et al. 2015a, A&A, 583, A76
Fernández-Trincado, J. G., Vivas, A. K., Mateu, C. E., et al. 2015b, A&A, 574, A15
Fernández-Trincado, J. G., Robin, A. C., Moreno, E., et al. 2016a, ApJ, 833, 132
Fernández-Trincado, J. G., Robin, A. C., Reylé, C., et al. 2016b, MNRAS, 461, 1404
Fernández-Trincado, J. G., Geisler, D., Moreno, E., et al. 2017a, in SF2A-2017: Proceedings of the Annual meeting of the French Society of Astronomy and Astrophysics, eds. C. Reylé, P. Di Matteo, F. Herpin, et al., 199
Fernández-Trincado, J. G., Zamora, O., García-Hernández, D. A., et al. 2017b, ApJ, 846, L2
Fernández-Trincado, J. G., Beers, T. C., Placco, V. M., et al. 2019a, MNRAS, submitted [arXiv:1904.05884]
Fernández-Trincado, J. G., Beers, T. C., Tang, B., et al. 2019b, MNRAS, submitted [arXiv:1904.05369]
Fernández-Trincado, J. G., Mennickent, R., Cabezas, M., et al. 2019c, A&A, submitted [arXiv:1902.10635]
Fernández-Trincado, J. G., Ortigoza-Urdaneta, M., Moreno, E., Pérez-Villegas, A., & Soto, M. 2019d, MNRAS, submitted [arXiv:1904.05370]
Fishlock, C. K., Karakas, A. I., Lugaro, M., & Yong, D. 2014, ApJ, 797, 44
Gaia Collaboration (Brown, A. G. A., et al.) 2018, A&A, 616, A1
García-Hernández, D. A., Mészáros, S., Monelli, M., et al. 2015, ApJ, 815, L4
García Pérez, A. E., Allende Prieto, C., Holtzman, J. A., et al. 2016, AJ, 151, 144
Gnedin, O. Y., & Ostriker, J. P. 1997, ApJ, 474, 223
Gratton, R., Sneden, C., & Carretta, E. 2004, ARA&A, 42, 385

Gratton, R. G., Lucatello, S., Bragaglia, A., et al. 2007, A&A, 464, 953
Gratton, R. G., Carretta, E., & Bragaglia, A. 2012, A&ARv, 20, 50
Grevesse, N., Scott, P., Asplund, M., & Sauval, A. J. 2015, A&A, 573, A27
Gunn, J. E., Siegmund, W. A., Mannery, E. J., et al. 2006, AJ, 131, 2332
Gustafsson, B., Edvardsson, B., Eriksson, K., et al. 2008, A&A, 486, 951
Harris, W. E. 1996, AJ, 112, 1487
Hasselquist, S., Shetrone, M., Cunha, K., et al. 2016, ApJ, 833, 81
Hawkins, K., Masseron, T., Jofré, P., et al. 2016, A&A, 594, A43
Heggie, D. C., Hut, P., & McMillan, S. L. W. 1996, ApJ, 467, 359
Hut, P. 1983, ApJ, 272, L29
Kerber, L. O., Nardiello, D., Ortolani, S., et al. 2018, ApJ, 853, 15
Küpper, A. H. W., Lane, R. R., & Heggie, D. C. 2012, MNRAS, 420, 2700
Lane, R. R., Küpper, A. H. W., & Heggie, D. C. 2012, MNRAS, 423, 2845
Lee, Y.-W., Kim, J. J., Johnson, C. I., et al. 2019, ApJ, 878, L2
Majewski, S. R., Schiavon, R. P., Frinchaboy, P. M., et al. 2017, AJ, 154, 94
Martell, S. L., & Grebel, E. K. 2010, A&A, 519, A14
Martell, S. L., Smolinski, J. P., Beers, T. C., & Grebel, E. K. 2011, A&A, 534, A136
Martell, S. L., Shetrone, M. D., Lucatello, S., et al. 2016, ApJ, 825, 146
Masseron, T., Merle, T., & Hawkins, K. 2016, Astrophysics Source Code Library [record ascl:1605.004]
Mészáros, S., Martell, S. L., Shetrone, M., et al. 2015, AJ, 149, 153
Mészáros, S., García-Hernández, D. A., Cassisi, S., et al. 2018, MNRAS, 475, 1633
Minniti, D., Lucas, P. W., Emerson, J. P., et al. 2010, New Astron., 15, 433
Muñoz, C., Villanova, S., Geisler, D., et al. 2017, A&A, 605, A12
Ness, M., Asplund, M., & Casey, A. R. 2014, MNRAS, 445, 2994
Nidever, D. L., Holtzman, J. A., Allende Prieto, C., et al. 2015, AJ, 150, 173
Pancino, E., Romano, D., Tang, B., et al. 2017, A&A, 601, A112
Pichardo, B., Moreno, E., Allen, C., et al. 2012, AJ, 143, 73
Pignatari, M., Gallino, R., Meynet, G., et al. 2008, ApJ, 687, L95
Recio-Blanco, A., Rojas-Arriagada, A., de Laverny, P., et al. 2017, A&A, 602, L14
Schiavon, R. P., Johnson, J. A., Frinchaboy, P. M., et al. 2017a, MNRAS, 466, 1010
Schiavon, R. P., Zamora, O., Carrera, R., et al. 2017b, MNRAS, 465, 501
Schultheis, M., Rojas-Arriagada, A., García Pérez, A. E., et al. 2017, A&A, 600, A14
Skrutskie, M. F., Cutri, R. M., Stiening, R., et al. 2006, AJ, 131, 1163
Smith, V. V., Cunha, K., Shetrone, M. D., et al. 2013, ApJ, 765, 16
Souto, D., Cunha, K., Smith, V., et al. 2016, ApJ, 830, 35
Tang, B., Cohen, R. E., Geisler, D., et al. 2017, MNRAS, 465, 19
Tang, B., Fernández-Trincado, J. G., Geisler, D., et al. 2018, ApJ, 855, 38
Tang, B., Liu, C., Fernández-Trincado, J. G., et al. 2019, ApJ, 871, 58
Vasiliev, E. 2019, MNRAS, 484, 2832
Ventura, P., García-Hernández, D. A., Dell'Agli, F., et al. 2016, ApJ, 831, L17
Wilson, J. C., Hearty, F., Skrutskie, M. F., et al. 2012, in Ground-based and Airborne Instrumentation for Astronomy IV, Proc. SPIE, 8446, 84460H
Zasowski, G., Johnson, J. A., Frinchaboy, P. M., et al. 2013, AJ, 146, 81
Zasowski, G., Cohen, R. E., Chojnowski, S. D., et al. 2017, AJ, 154, 198

[1] Instituto de Astronomía y Ciencias Planetarias, Universidad de Atacama, Copayapu 485, Copiapó, Chile
e-mail: jfernandez@obs-besancon.fr
[2] Institut Utinam, CNRS UMR 6213, Université Bourgogne-Franche-Comté, OSU THETA Franche-Comté, Observatoire de Besançon, BP 1615, 25010 Besançon Cedex, France
[3] Departamento de Astronomía, Casilla 160-C, Universidad de Concepción, Concepción, Chile
[4] Instituto de Astrofísica de Canarias, Vía Láctea s/n, 38205 La Laguna, Tenerife, Spain
[5] Departamento de Astrofísica, Universidad de La Laguna (ULL), 38206 La Laguna, Tenerife, Spain
[6] Observatório Nacional, Rua Gal. José Cristino 77, 20921-400 Rio de Janeiro, Brazil
[7] Departamento de Física, Universidade Federal de Sergipe, Av. Marechal Rondon, s/n, 49000-000 São Cristóvão, SE, Brazil
[8] Space Telescope Science Institute, 3700 San Martin Dr, Baltimore, MD 21218, USA
[9] Astrophysics Research Institute, Liverpool John Moores University, 146 Brownlow Hill, Liverpool L3 5RF, UK
[10] ELTE Gothard Astrophysical Observatory, Szent Imre Herceg st., 9704 Szombathely, Hungary
[11] Steward Observatory, University of Arizona, 933 North Cherry Avenue, Tucson, AZ 85721, USA
[12] New Mexico State University, Las Cruces, NM 88003, USA
[13] University of Texas at Austin, McDonald Observatory, Fort Davis, TX 79734, USA
[14] School of Physics and Astronomy, Sun Yat-sen University, Zhuhai 519082, PR China
[15] Departamento de Física, Facultad de Ciencias, Universidad de La Serena, Cisternas 1200, La Serena, Chile
[16] Instituto de Investigación Multidisciplinario en Ciencia y Tecnología, Universidad de La Serena, Avenida Raúl Bitrán s/n, La Serena, Chile
[17] Departamento de Fisica, Facultad de Ciencias Exactas, Universidad Andres Bello, Av. Fernandez Concha 700, Las Condes, Santiago, Chile
[18] Instituto Milenio de Astrofisica, Santiago, Chile
[19] Vatican Observatory, 00120 Vatican City State, Italy
[20] Centro de Astronomía (CITEVA), Universidad de Antofagasta, Av. Angamos 601, Antofagasta, Chile
[21] Consejo Superior de Investigaciones Científicas, Spain
[22] Department of Physics and JINA Center for the Evolution of the Elements, University of Notre Dame, Notre Dame, IN 46556, USA
[23] Department of Astronomy, University of Washington, Seattle, WA 98195, USA
[24] Department of Physics & Astronomy, University of Utah, Salt Lake City, UT 84112, USA
[25] Laboratoire Lagrange, Université Côte d'Azur, Observatoire de la Côte d'Azur, CNRS, Blvd de l'Observatoire, 06304 Nice, France
[26] Department of Astronomy, University of Virginia, Charlottesville, VA 22903, USA
[27] Instituto de Astrofśica, Pontificia Universidad Católica de Chile, Av. Vicuna Mackenna 4860, 782-0436 Macul, Santiago, Chile
[28] Universidad de Chile, Av. Libertador Bernardo O'Higgins 1058, Santiago, Chile
[29] Department of Physics & Astronomy, Vanderbilt University, Nashville, TN 37235, USA
[30] Department of Physics, University of California, San Diego, CA 92093, USA
[31] Department of Astronomy and Astrophysics, The Pennsylvania State University, University Park, PA 16802, USA

Appendix A: Line-by-line abundance determination

Table A.1. Line-by-line abundance information for every possible member of NGC 6522.

Element	λ^{air} (Å)	2M18032356−3001588	2M18034052−3003281	2M18033965−3000521	2M18033819−3000515	2M18033660−3002164
Fe I	15194.492	6.23	–	6.43	6.49	–
	15207.526	6.15	6.36	6.50	6.51	6.17
	15395.718	6.35	6.49	6.52	–	6.38
	15490.339	6.24	6.42	6.52	6.58	–
	15648.510	6.23	6.38	6.46	6.50	–
	15964.867	6.31	6.57	6.44	6.42	6.49
	16040.657	6.20	6.54	6.39	6.42	6.38
	16153.247	6.25	6.50	6.45	6.50	6.46
	16165.032	6.23	6.57	6.42	6.43	6.35
$\langle$A(Fe)$\rangle \pm \sigma$		6.25 ± 0.05	6.48 ± 0.08	6.46 ± 0.04	6.48 ± 0.05	6.37 ± 0.10
Al I	16719.0	5.54	6.41	5.75	6.16	5.68
	16750.0	5.56	6.32	5.78	6.09	–
	16763.0	–	6.26	–	6.26	–
$\langle$A(Al)$\rangle \pm \sigma$		5.55 ± 0.01	6.33 ± 0.06	5.77 ± 0.02	6.17 ± 0.07	5.68
Mg I	15740.7	6.53	6.63	6.58	6.64	6.99
	15748.9	6.52	6.68	6.59	6.68	6.72
	15765.8	6.41	6.53	–	6.49	6.63
$\langle$A(Mg)$\rangle \pm \sigma$		6.49 ± 0.05	6.61 ± 0.06	6.59 ± 0.05	6.60 ± 0.08	6.78 ± 0.15
Si I	15361.1	–	–	–	–	–
	15376.8	–	–	–	–	–
	15557.8	6.62	6.86	–	6.68	–
	15884.5	6.39	6.76	6.63	6.63	–
	15960.1	6.53	7.10	6.65	6.67	6.82
	16060.0	6.64	6.97	6.82	6.71	–
	16094.8	6.61	6.92	6.72	6.79	6.66
	16129.0	–	–	–	–	–
	16163.7	6.71	7.00	–	6.79	–
	16170.2	–	–	–	–	–
	16215.7	6.53	6.92	6.70	6.68	–
	16241.8	–	6.83	6.65	6.63	–
	16680.8	6.56	6.88	6.74	6.64	7.33
	16828.2	6.74	6.89	–	6.89	–
$\langle$A(Si)$\rangle \pm \sigma$		6.59 ± 0.10	6.91 ± 0.09	6.70 ± 0.06	6.71 ± 0.08	6.94 ± 0.29
Ce II	15277.65	–	–	–	–	–
	15784.75	0.48	–	–	–	–
	15958.40	0.50	–	–	0.88	–
	15977.12	–	–	–	0.83	–
	16327.32	–	–	–	–	–
	16376.48	0.40	–	–	0.81	–
	16595.18	0.50	–	–	0.84	–
	16722.51	–	–	–	–	–
$\langle$A(Ce)$\rangle \pm \sigma$		0.47 ± 0.04	–	–	0.84 ± 0.03	–
^{12}C from ^{12}C^{16}O lines	15 774−15 787	6.67	–	–	7.10	–
	15 976−16 000	6.75	7.20	7.15	7.13	–
	16 183−16 196	6.71	7.16	7.07	7.04	–
$\langle$A(C)$\rangle \pm \sigma$		6.71 ± 0.03	7.18 ± 0.02	7.11 ± 0.04	7.09 ± 0.04	–
^{14}N from ^{12}C^{14}N lines	15260.	7.88	8.01	–	8.14	–
	15322.	7.97	8.08	7.83	8.18	–
	15397.	–	–	–	8.06	–
	15332.	7.86	8.10	7.88	8.10	7.70
	15410.	7.88	8.11	7.87	8.13	–
	15447.	7.82	7.80	–	8.09	–
	15466.	7.78	7.89	7.78	8.05	7.95
	15472.	7.92	8.04	–	8.17	–
	15482.	7.81	8.04	7.76	8.06	–
$\langle$A(N)$\rangle \pm \sigma$		7.87 ± 0.06	8.01 ± 0.10	7.82 ± 0.05	8.11 ± 0.05	7.83 ± 0.13
^{16}O from ^{16}OH lines	15278.524	7.93	–	–	7.87	–
	15281.052	7.86	8.02	–	8.10	–
	15390.8	7.81	–	7.97	8.02	–
	15568.780	7.95	8.06	–	8.04	–
	16190.132	7.76	–	7.94	7.94	–
	16192.130	7.80	–	–	7.98	–
$\langle$A(O)$\rangle \pm \sigma$		7.85 ± 0.07	8.04 ± 0.02	7.96 ± 0.02	7.99 ± 0.07	–